Kimberlite Volcanology: Transport, Ascent, and Eruption

J. Kelly Russell[1], R. Stephen J. Sparks[2], and Janine L. Kavanagh[3]

ABSTRACT

Kimberlite rocks and deposits are the eruption products of volatile-rich, silica-poor ultrabasic magmas that originate as small-degree mantle melts at depths in excess of 200 km. Many kimberlites are emplaced as subsurface cylindrical-to-conical pipes and associated sills and dykes. Surficial volcanic deposits of kimberlite are rare. Although kimberlite magmas have distinctive chemical and physical properties, their eruption styles, intensities and durations are similar to conventional volcanoes. Rates of magma ascent and transport through the cratonic lithosphere are informed by mantle cargo entrained by kimberlite, by the geometries of kimberlite dykes exposed in diamond mines, and by laboratory-based studies of dyke mechanics. Outstanding questions concern the mechanisms that trigger and control the rates of kimberlite magmatism.

Keywords: kimberlite, volcanology, transport, dykes, eruption, xenolith, ascent

INTRODUCTION

Kimberlite magmas have the deepest origins of all terrestrial magmas (>200 km). They transport substantial loads (>25 vol%) of dense mantle-derived rocks and minerals, including diamond, through the mantle lithosphere to the Earth's surface. Ascent rates estimated from entrainment of large (radii > 10 cm) mantle xenoliths, preservation of mantle temperatures in xenoliths, dehydration rims on olivine xenocrysts, dissolution rates of mantle minerals, and combustion or graphitization rates of diamond are as fast or faster (~1 to 10's $m \cdot s^{-1}$) than those ascribed to other mantle-derived magmas (e.g., Eggler 1989; Sparks 2013). Total transit times through ~150–200 km of relatively cool cratonic mantle lithosphere are estimated at <10 h to ~2 days. Rise rates could be lower if kimberlite magmas are assumed to have significant yield strength. However, to entrain the deepest-seated

[1] University of British Columbia
Vancouver, Canada, V7W-2S1
E-mail: krussell@eoas.ubc.ca
[2] Bristol University
Bristol, UK, BS8 1RJ
E-mail: steve.sparks@bristol.ac.uk
[3] University of Liverpool
Liverpool, UK, L69 3GP
E-mail: Janine.Kavanagh@liverpool.ac.uk

peridotite xenoliths and suppress the settling out of 10–20 cm xenoliths requires that the initial melts must have high-to-unrealistic yield strengths (1,000–2,000 Pa) (Spera 1984).

There have been no historic eruptions of kimberlite volcanoes to constrain the styles, intensities and durations of eruption. Much of our understanding derives from studies of kimberlite deposits preserved in subsurface bodies (FIG. 1) for which diamond mining operations have contributed a unique and critical body of knowledge (Cas et al. 2008; Field et al. 2008). Remnants of the original volcanoes and surficial kimberlite deposits are less common but, where preserved (e.g., Fort à la Corne in Canada; Igwisi Hills volcanoes in Tanzania), they directly inform on kimberlite volcanic landforms and the nature of the intra- and extra-crater deposits.

Here, we provide a summary of emerging ideas concerning the transport, ascent, and eruption of kimberlite magma. We begin with near-surface processes, for which we have abundant geological observations, and move deeper to where data becomes scarcer Important supporting data sources are at http://elementsmagazine.org/supplements/.

KIMBERLITE MELT AND MAGMA

Kimberlite is a rock type found at and near the Earth's surface and is defined on the basis of mineralogy and texture, including the abundance (~15–40 vol%) of mantle-derived xenoliths and xenocrysts (Mitchell et al. 2019 this issue). The nature and composition of the primary kimberlite melts entering the cratonic mantle lithosphere (i.e., *proto-kimberlite*) are obscured by the entrainment of, and chemical interaction with, these large volumes of xenolithic material. Kimberlite magmas are particularly complicated because their componentry, character, and properties may be highly transient and evolve during ascent. Furthermore, the ultrabasic composition and age of kimberlites make them susceptible to post-emplacement alteration (i.e., serpentinization) and textural modification that will involve a loss of primary pore space (Cas et al. 2008; Field et al. 2008; Brown et al. 2012).

Melt compositions estimated from kimberlites that reached the Earth's surface or the shallow crust are generally SiO_2-poor, MgO-rich, and are thought to be volatile-rich, being dominated by CO_2 (<15 wt%) with subordinate H_2O (e.g., Price et al. 2000; Sparks et al. 2006). Calculations and experiments suggest densities of 2,600–3,000 $kg \cdot m^{-3}$ and melt viscosities between 0.1 Pa·s and 3 Pa·s at mantle conditions. However, primary melt entering the base of the cratonic mantle lithosphere may well be more carbonatitic ($\lesssim$ 10–17 wt% SiO_2) and evolve chemically, during ascent, to erupt as "kimberlite". The properties of the proto-kimberlite melt are, therefore, likely to be different. The work by Dobson et al. (1996) on synthetic Ca–Mg-carbonate melts between 1,350 °C and 1,600 °C and ~ 5 GPa indicates

that proto-kimberlite melts could be 5–10% less dense (2,300–2,800 kg·m^{-3}) and two orders of magnitude less viscous (6–36 × 10^{-3} Pa·s) than values estimated for erupted kimberlite.

KIMBERLITE VOLCANOES

The classic composite model for kimberlite volcanoes comprises crater, pipe (e.g., diatreme) and shallow seated (hypabyssal) intrusive bodies. However, individual kimberlites are diverse and can range in geometry from champagne glass shaped craters (e.g., Fort à la Corne field) to deeply excavated narrow pipes (e.g., Lac de Gras field). The pronounced differences in geometry correlate with host-rock geology, eruptive environment, as well as present-day erosion levels (Field and Scott Smith 1999; Field et al. 2008).

Kimberlite Crater and Surficial Deposits

Remnants of kimberlite volcanoes preserve deposits of pyroclastic fallout, pyroclastic density currents, re-sedimented kimberlite, and lavas such as described at Fort à la Corne (Pittari et al. 2008; Lefebvre and Kurszlaukis 2008; Scott Smith 2008) or the Igwisi Hills volcanoes (Brown et al. 2012). These occurrences suggest there are a diversity of eruption environments (subaerial vs subaqueous), styles (explosive vs effusive), and types of explosivity (magmatic vs phreatomagmatic) and also testify to the range of complex processes that fill the craters and the pipes.

The Fort à la Corne kimberlite field comprises >70 bodies of volcaniclastic kimberlite hosted within a contemporaneous non-volcanic sedimentary succession. The Fort à la Corne kimberlites erupted explosively from low-to-negative surface relief vents through weak sedimentary host rocks and into a marine setting, forming diverse pyroclastic and volcaniclastic extra-crater and crater-filling deposits. The environmental setting suggests explosive eruptions controlled by shallow phreatomagmatic fragmentation (e.g., Lorenz 1975) which, when combined with the weak surface rocks, favoured formation of wide, near-surface craters and inhibited the excavation of deep vertical pipes (Field and Scott Smith 1999). Whether the large, shallow, bowl-shaped craters (e.g., Fort à la Corne) are underlain by narrow vertical pipes within basement rocks remains untested.

The Holocene Igwisi Hills volcanoes in Tanzania are the youngest known kimberlites (~10 ka) (Brown et al. 2012). Three vents with eroded low-relief pyroclastic cones (FIG. 1A), craters and extra-crater lavas are preserved and provide unique insights into kimberlite eruption dynamics. The volume of surficial pyroclastic deposits and lava is ~3.5 × 10^{6} m^{3}. The deposits comprise layered fallout of juvenile pyroclasts that can be either scoriaceous or dense. The reconstructed three-stage eruption process is possibly as follows: 1) an initial

phase of explosive crater and conduit excavation, as recorded by lithic clast-bearing tuffs; 2) pyroclastic cone formation from a mildly explosive, unsteady, Strombolian eruption; 3) a late-stage effusion to form a lava lake and small volumes of dense to poorly vesicular, viscous, extra-crater lavas (FIG. 1A). The explosive eruptions spanned days to several months; the effusive phase hours to days. This is a common type of eruptive sequence and duration and has been observed at many monogenetic basaltic volcanoes.

Kimberlite Pipe Infill

Many kimberlite deposits occur in deep, subsurface pipes, or diatremes, that feature steep (75° to vertical), smooth, striated walls (Cas et al. 2008) and "root zones" of associated sills and dykes (FIG. 1B). These pipes are the remnant conduits and feeders to subaerial kimberlite volcanoes (Field and Scott Smith 1999; Field et al. 2008).

Contacts between conduit wall rocks and infilling deposits are characteristically sharp, and contacts between units can be near vertical to horizontal (FIG. 1B). Aided by the lithofacies concept, within-pipe deposits are defined by distinctive geological, structural and textural features, such as bedding, grain size, clast lithology and sorting (see Cas et al. 2008). In some instances, deposits within pipes can derive from later or synchronous eruptions of neighbouring volcanoes, e.g., at the Fort à la Corne field (Lefebvre and Kurszlaukis 2008) or the Lac de Gras field (Moss et al. 2008).

The complexity within kimberlite pipes reflects multistage eruptions rather than single catastrophic explosions. Most kimberlite deposits can be divided into two types: volcaniclastic or coherent (Sparks et al. 2006; Cas et al. 2008; Sparks 2013). Volcaniclastic kimberlite can be in the form of massive volcaniclastic kimberlite or variably layered volcaniclastic kimberlite, and include apparently coherent kimberlite deposits (FIG. 1B). The apparently coherent kimberlite–type deposits have pyroclastic origins but form dense and coherent deposits (e.g., Brown et al. 2008), including clastogenic lavas (e.g., the Victor kimberlite in Canada) and welded pyroclastic kimberlite (e.g., Muskox and Jericho kimberlites of Canada), both of which are indicative of relatively high emplacement temperatures of 700–950 °C (Pell et al. 2018).

Intrusive Kimberlite Deposits

Coherent kimberlite mainly occurs as shallow intrusive dykes and sills (i.e., hypabyssal kimberlite) either in the root zone of pipes or as late intrusions into the pipe infill (FIG. 1B). Some root zones to kimberlite pipes feature irregular vertical lobes of intrusive kimberlite that have no apparent connection to the surface. These "blind" intrusions (Field and Scott Smith 1999; Field et al. 2008) comprise coherent or volcaniclastic (breccia) kimberlite and

are usually connected laterally to the main kimberlite body. They commonly contain xenoliths of local wall rocks and have textures and mineralogy that suggest emplacement from volatile-rich magma. One possibility is that such blind re-entrants of kimberlite result from large pressure fluctuations in the pipe and root zone due to breakthrough of the main pipe (McCallum 1976) or from downward widening of the conduit (Sparks 2006).

Recent studies of the Kelvin and Faraday kimberlites (Canada) describe complexly interlayered, xenolith-rich, coherent and volcaniclastic kimberlite within shallow-dipping tubular-shaped dykes (Barnett et al. 2018). These enigmatic bodies (or "chonoliths") pose major mechanical issues because their shapes are inconsistent with simple intrusion accommodated by elastic deformation of wall rocks. Instead, their geometry suggests removal of host rock to create space thereby allowing flow and replacement by kimberlite (be it coherent or volcaniclastic). Although it is unclear whether these are part of an "open" volcanic feeder system or are "closed" blind intrusions, the xenolith-rich volcaniclastic deposits clearly suggest explosive magmatic fragmentation.

RECONSTRUCTING KIMBERLITE ERUPTIONS

Reconstructing eruption history, style and duration is relatively straightforward when the kimberlite volcano and its deposits are preserved, such as at Fort à la Corne or the Igwisi Hills volcanoes. It is a challenge to do so when the volcano and its crater facies deposits have been removed (e.g., Lac de Gras field) (FIG. 1B).

The A418 pipe (Northwest Territories, Canada) illustrates the unique approach required to reconstruct kimberlite eruption history solely from subsurface pipe deposits (i.e., volcanic conduits) (Cas et al. 2008). At the present-day surface, estimated to be ~50–200 m below the original surface, A418 has a diameter of ~125 m (Porritt et al. 2013). The cylindrical pipe tapers down to ~50 m in diameter at ~600 m depth (FIG. 1B) before transitioning to a root zone of narrow dykes. Pipe formation involved fragmentation and excavation of near-surface wall rocks driven by explosive release of magmatic volatiles and, sometimes, augmented by explosive interactions with ground water (Lorenz 1975; Sparks 2013). The volume of excavated crustal wall rock at A418 is ~6–8 × 10^6 m^3. Unlike the Igwisi Hills volcanoes, there are no deposits that record the pipe excavation phase of eruption. However, conservative estimates based on entrainment of ~5–10 vol% wall rock lithics suggest a highly energetic eruption of 0.1–0.2 km^3 (dense-rock equivalent) of kimberlite. Assuming a range of sustained, steady exit-velocities of 100–400 $m \cdot s^{-1}$, capable of ejecting lithics ~7–10 cm in diameter, and a minimum initial pipe diameter (D ~10 m), the pipe excavation phase would last a minimum of ~2.5–36 h for a gas-charged (~70–90 vol%) eruptive flux. Post-pipe

excavation eruptive activity is represented by the deposits that infill the excavated subsurface pipe (FIG. 1B). These suggest a less energetic pulsatory, phreatomagmatic phase of eruption, expressed by repeated sequences of inwardly dipping, finely bedded pyroclastic surge deposits containing abundant accretionary lapilli (Lorenz 1975; Porritt et al. 2013). The last phase of activity involved intrusion of coherent kimberlite into unconsolidated pipe infill (FIG. 1B).

ENTRAINMENT AND MODIFICATION OF MANTLE CARGO

One of the defining characteristics of kimberlite is the high proportion of entrained and transported mantle-derived material (e.g., peridotite, eclogite) that represents sampling of the entire (i.e., ~150–200 km) cratonic mantle lithosphere. Xenoliths are typically 1–25 cm, but can be ~1 m in diameter (FIGS. 2A, 2B). Xenocrysts from disaggregated xenoliths (FIGS. 2C–F) are dominated by olivine but include clinopyroxene, garnet and ilmenite. Notably, xenocrystic orthopyroxene is rare relative to its abundance in peridotite (FIG. 2E) (Mitchell et al. 2019 this issue). Xenoliths and xenocrystic olivine grains can be moderately sub-rounded to well-rounded (FIG. 2A–D).

The abundant xenocrysts result from the high ascent rates of the kimberlite magma. Consequent rapid decompression increases internal stresses within xenoliths inducing tensile failure to produce smaller xenoliths and xenocrysts (Brett et al. 2015). The continuous entrainment, disaggregation and partial assimilation of mantle xenoliths during ascent results in a physically and chemically evolving kimberlite magma.

ASSIMILATION, VOLATILES AND BUOYANCY

Rapid ascent of kimberlite requires substantial buoyancy and magma overpressure but is hindered by entrainment of large volumes of dense mantle material. Most models for kimberlite ascent invoke an exsolved CO_2–H_2O fluid phase to reduce the magma's bulk density. Brey and Ryabchikov (1994), for example, suggested a pressure-induced drop in CO_2 solubility at depths corresponding to ~4–5 GPa driving buoyancy-enhancing exsolution of CO_2 fluid within the "diamond window".

Russell et al. (2012) proposed a new "chemical" mechanism for continuous and spontaneous exsolution of CO_2 fluid to support rapid ascent (FIG. 3). They argue that the proto-kimberlite magma entering the base of the cratonic mantle lithosphere was more carbonatitic in composition (see Kamenetsky 2016). The proto-kimberlite assimilates silicate minerals liberated from xenoliths, so causing SiO_2-enrichment of the melt that, in turn, decreases CO_2 solubility, thereby resulting in spontaneous CO_2 exsolution (FIGS. 3A) (Russell et al. 2012).

The "missing" orthopyroxene (see above) is ascribed to its preferential and rapid assimilation relative to other mantle phases (FIG. 2E). Fuelled by exsolution and an increase in buoyancy, the magma accelerates upward for as long as the volatiles remain coupled to the melt. Assimilation ultimately produces a "kimberlite" melt that attains olivine saturation in the shallow mantle and crust (FIGS. 3A, 3C), resulting in the crystallization of olivine microphenocrysts and in olivine overgrowths on partially resorbed xenocrysts (FIG. 2F) (Brett et al. 2015; Mitchell et al. 2019 this issue). Additional evidence for early and sustained dissolution of mantle silicates is expressed by the irregular, embayed anhedral shapes preserved in cores to many olivine xenocrysts (FIG. 2F).

The Russell et al. (2012) model postulates early, deep-seated exsolution of CO_2-rich fluids long before any significant decrease in lithostatic pressure occurs: potentially, as soon as proto-kimberlite enters the lithosphere (~6 GPa) (FIG. 3A-C). Recently, this hypothesis was tested experimentally, constraining the assimilation-induced exsolution event to ≤ 3.5 GPa, coincident with the top of the "diamond window" (Stone and Luth 2016). Given the entrainment of material from the deepest part of the cratonic mantle lithosphere (i.e., 150–210 km, or 5–7 GPa), this pressure limit suggests an, as yet, unidentified, deeper buoyancy mechanism, possibly involving very low-density, carbonatitic proto-kimberlite melts.

KIMBERLITE TRANSPORT IN DYKES

Magma is transported from source to surface via fractures (dykes) to feed volcanic eruptions. Exposures of kimberlite dykes and sills are typically at depths of 1 km to 3 km and observations on 2-D and 3-D sections show dykes to be segmented, en echelon, and typically thin (~0.6 m) with tapered margins (Kavanagh 2018).

Dyke Mechanics

The dynamics of dyke propagation can be described by theory for a fluid-filled fracture intruding an elastic material. This theory constrains the overall 3-D geometry of kimberlite dykes and identifies the specific conditions for dyke-fed kimberlite eruptions. The main driver for dyke ascent is magma buoyancy, which at 300 MPa is particularly large for kimberlite dykes. Initially, the dyke has a penny-shape and is elliptical in cross-section, but this quickly narrows in width and develops a tear-drop cross-section during ascent (see FIG. 4) due to the large and increasing density contrast between the magma and its surroundings during ascent.

The overall volume of a 150 km long, 1 m thick and ~400 m wide dyke would be ~5×10^7 m^3, which is ~10 times larger than the volume of material erupted by the Igwisi Hills

volcanoes but 5–10 times smaller than that erupted by A418 (see above). However, the erupted kimberlite deposits represent only those magmas that have the favourable properties necessary to reach the shallow crust (<5 km depth): >80% of dykes never erupt (Kavanagh 2018).

Dyke Damage Zone and the Volatile-Rich Tip

The propagation pathway of dykes is strongly influenced by the ambient stress field and by the mechanical heterogeneities in the host rock. Stress concentrations at the tip and between dyke segments produce a "damage zone" as the walls are pushed apart by magma overpressure (FIG. 4). The damage zone comprises a series of closely spaced dyke-parallel fractures and breccia between segments, envelopes the full dyke geometry, and is the main source of the entrained xenoliths (FIG. 4).

The dyke tip region is expected to feature a narrow, low-density volatile-filled pocket (FIG. 4). The volatiles can be coupled to the magma or may separate and ascend ahead of the dyke causing chemical conditioning and weakening of wall rocks (i.e., fenitization) and potential precursory volatile-rich phreatic eruptions (McCallum 1976). Alternatively, such degassing may raise the effective liquidus temperature, thereby inducing crystallisation, increased magma viscosity and, ultimately, dyke arrest.

Dyke Velocity, Magma Flow and Eruption Dynamics

The velocity of magma within rising dykes varies spatially and temporally (FIG. 4) and is highest in the central part of a dyke (Kavanagh et al. 2018). Low-viscosity magmas, such as kimberlite, develop a high-velocity magma "jet" within the dyke which can preferentially transport mantle xenoliths and enhance mixing. Moreover, turbulent flow in the volatile-filled head of the dyke provides an environment for efficient pre-eruption milling of xenoliths and xenocrysts (FIG. 2) (Brett et al. 2015; Jones et al. 2019). Competition between turbulence and particle settling ultimately dictates whether dense mantle cargo is entrained or sedimented in the dyke (FIG. 4).

Following Sparks et al. (2006), and using proto-kimberlite properties introduced above, we calculated[4] a characteristic turbulent magma velocity of ~20–90 m/s . This suggests that a minimum discharge rate from a 1 m thick and ~400 m wide dyke is on the order of ~10,000 m^3/s, which is typical of Strombolian to sub-Plinian explosive intensities (comparable to the 1980 eruption of Mount St. Helens, USA) and consistent with inferences from kimberlite

[4] For specifics regarding these calculations, see the supplementary content found at http://elementsmagazine.org/supplements.

deposits. The onset of dyke eruption will be from a short fissure that, due to the penny-shaped 3-D dyke geometry, is much narrower than the dyke in the sub-surface. As the dyke erupts, the source may become depressurised and unstable, potentially inducing further magma ascent via new or existing dykes. The pressure release upon eruption causes elastic recovery of the host rock, closing up the kimberlite dyke from depth to the surface.

At the surface, many kimberlite volcanoes or pipes are associated with precursor dykes, as seen for the Igwisi Hills volcanoes (Brown 2012), the Lac de Gras field (Moss et al. 2008) or the Jericho kimberlite (Price et al. 2002). This type of dyke occurrence suggests that dyke transport of kimberlite magma continues almost to the Earth's surface. The initial dyke-fed eruptions appear to become rapidly localized (e.g., Jones et al. 2017), thereby focussing the main eruptive flux and forming point-source volcanoes and pipes. Localization can cause a massive change in eruption velocity (for a constant flux) that, under the right conditions (e.g., deep fragmentation, crystalline wall rocks), facilitates the excavation of deep vertical pipes. The excavation of kimberlite pipes, as in other volcanic conduits, is driven by large pressure fluctuations during explosive flow (Costa et al. 2009). Large overpressures can be caused by volatile exsolution or the heating of groundwater and provide a means of excavating near-surface craters and also contribute to pipe deepening. Conversely, large underpressures will likely develop as fragmentation levels deepen, thereby creating conditions for tensile wall-rock failures and conduit widening (Sparks 2013).

KIMBERLITE PRODUCTION AND ASCENT TRIGGERING

Kimberlites represent monogenetic volcanic fields and show clustering in both space and time. Kimberlite volcanoes are typically widely distributed on a craton-scale, but also show strong spatial clustering with localised concentrations and elongate footprints at scales of tens of kilometres, suggesting control by either basal lithosphere topography or major lithospheric structures.

Temporal clustering has been recognised in all kimberlite provinces (Heaman et al. 2019 this issue). Individual pulses of kimberlite volcanism that span between 10 My and 20 My are common, and periods without kimberlite volcanism can have durations >100 My. Some kimberlite data suggest hot spot trails lasting many tens of millions of years. Minimum rates of kimberlite eruption assessed from geochronology data and from mapping of vents and dykes vary from ≥ 1 event per 0.3 My (southern Africa and the Lac de Gras field) to 1 event per 0.08 My (Fort à la Corne, which has 169 bodies emplaced over 13 My).

These observations suggest that kimberlite melts can be generated on a craton scale (~1,000 km) at the base of the lithosphere but that individual melt sources have a scale of 10 km to 100 km. Conditions for melt ascent develop over time periods of ~100 ky. We have applied models[5] of melt segregation and accumulation to the consideration of kimberlite production wherein a melt-rich layer segregated from the more permeable asthenosphere accumulates at the base of the lithosphere. This melt layer is buoyant relative to the overlying lithosphere and so is unstable (i.e. Rayleigh–Taylor instabilities develop[6]); instabilities grow with a characteristic timescale that depends on the ratio of the mantle lithosphere viscosity, the buoyancy of the melt, and the width of the melt layer (Seropian et al. 2018). As the instability grows, the pressure difference and strain rate in tension in the mantle at the melt–mantle boundary increases, causing conditions for dyke nucleation and propagation to develop. The potential melt volume will depend on layer width and melt layer growth rate as supplied by porous melt flow in the asthenosphere.

Our model results indicate that time scales of episodic kimberlite ascent for layers with widths of 300 m and 30 km are in the range 6×10^4 to 6×10^5 years, respectively. Melt accumulation rates ($\dot{h}$) of 10^{-5} m/year, taken as representative of asthenospheric melt segregation, imply a corresponding thicknesses (h) of 0.68 m and 6.8 m and accumulated melt volumes of 48 km^3 and 4.8 km^3 at these times. These calculations give timescales consistent with observations, but volumes are typically larger by at least an order of magnitude more than the volumes of individual kimberlites (3.5×10^{-3} to 1 km^3). The latter discrepancy might be explained if much of the kimberlite magma stalls to form intrusions within the overlying mantle lithosphere rather than successfully ascending to erupt. More generally, the difference between the calculated magma volumes versus the field observation volumes reflects uncertainties in the choice of model parameters and the conditions for dyke initiation.

SUMMARY

The styles, intensities, and durations of all volcanic eruptions reflect the chemical and physical properties of the magmas. Kimberlite eruptions are diverse and span most of the styles observed for other conventional magmas. The nature, composition and properties of kimberlite magmas are transient and evolve during ascent. In essence, the properties of the

[5] For details about these models, see the supplementary content found at http://elementsmagazine.org/supplements.

[6] For details about these models, see the supplementary content found at http://elementsmagazine.org/supplements.

kimberlite magmas that erupt are inherited during their upward transport (via a dyke mechanism) by processes such as xenolith entrainment, fluid exsolution, mineral assimilation and crystallization. However, the relative timings of these competing processes remain unresolved.

Kimberlite magmas erupt explosively, indicating the presence of a high-volume fraction of exsolved magmatic fluids. Erupted kimberlite deposits also contain abundant, and often large (>0.5 m), dense xenoliths from the deep mantle. These observations raise important unresolved questions concerning the extent and mechanisms of coupling between the kimberlite melt, mantle xenoliths and large volumes of low-density CO_2-dominated fluids released during dyke ascent. The unresolved question of "Where does fluid exsolution start?" is critical for understanding kimberlite buoyancy and ascent rates.

ACKNOWLEDGEMENTS

We thank Rich Brown and an anonymous referee for their critical reviews. We also greatly benefitted from discussions with Mathew Field. Support derives from NSERC (JKR), Leverhulme Emeritus Fellowships (RSJS), and the Royal Society (JLK).

REFERENCES

Barnett W and 5 coauthors (2018) Kelvin and Faraday kimberlite emplacement geometries and implications for subterranean magmatic processes. Mineralogy and Petrology 112 (Supplement 2): 447-462

Brett RC, Russell JK, Andrews GDM, Jones TJ (2015) The ascent of kimberlite: insights from olivine. Earth and Planetary Science Letters 424: 119-131

Brey GP, Ryabchikov ID (1994) Carbon-dioxide in strongly silica undersaturated melts and origin of kimberlite magmas. Neues Jahrbuch für Mineralogie - Monatshefte 10: 449-463

Brown RJ and 7 coauthors (2012) Eruption of kimberlite magmas: physical volcanology, geomorphology and age of the youngest kimberlitic volcanoes known on earth (the Upper Pleistocene/Holocene Igwisi Hills volcanoes, Tanzania). Bulletin of volcanology 74: 1621-1643

Brown RJ, Buse B, Sparks RSJ, Field M (2008) On the welding of pyroclasts from very low-viscosity magmas: examples from kimberlite volcanoes. Journal of Geology 116: 354-374

Costa A, Sparks, RSJ, Macedonio G, Melnik O (2009) Effects of wall-rock elasticity on magma flow in dykes during explosive eruptions. Earth and Planetary Science Letters 288: 455-462

Eggler DH (1989) Kimberlites; how do they form? In: Ross J (ed) Kimberlites and Related Rocks. Volume 1. Their Composition, Occurrence, Origin and Emplacement.

Proceedings of the Fourth International Kimberlite Conference, Geological Society of Australia Special Publication 14, pp 489-504

Field M, Stiefenhofer J, Robey J, Kurszlaukis S (2008) Kimberlite-hosted diamond deposits of southern Africa: a review. Ore Geology Reviews 34: 33-75

Field M, Scott Smith BH (1999) Contrasting geology and near-surface emplacement of kimberlite pipes in southern Africa and Canada. In: Gurney JJ, Gurney JL, Pascoe MD, Richardson, SH (eds) Proceedings of the VIIth International Kimberlite Conference. Red Roof Design, Cape Town, pp 214-237

Kimberlites through time. Elements 15: XXX-XXX

Jones TJ, Russell JK, Sasse D (2019) Modification of mantle cargo by turbulent ascent of kimberlite. Frontiers in Earth Science doi: 10.3389/feart.2019.00134

Jones TJ, Llewellin EW, Houghton BF, Brown RJ, Vye-Brown C (2017) Proximal lava drainage controls on basaltic fissure eruption dynamics. Bulletin of Volcanology 79 doi: 10.1007/s00445-017-1164-2

Kamenetsky VS (2016) Comment on: "The ascent of kimberlite: insights from olivine" by Brett R.C. et al. [Earth Planet. Sci. Lett. 424 (2015) 119-131]. Earth and Planetary Science Letters 440: 187-189

Kavanagh JL and 6 coauthors (2018) Challenging dyke ascent models using novel laboratory experiments: implications for reinterpreting evidence of magma ascent and volcanism. Journal of Volcanology and Geothermal Research 354: 87-101

Lefebvre N, Kurszlaukis S (2008) Contrasting eruption styles of the 147 Kimberlite, Fort à la Corne, Saskatchewan, Canada. Journal of Volcanology and Geothermal Research 174: 171-185

Lorenz V (1975) Formation of phreatomagmatic maar-diatreme volcanoes and its relevance to kimberlite diatremes. Physics and Chemistry of the Earth 9: 17-29

McCallum ME (1976) An emplacement model to explain contrasting mineral assemblages in adjacent kimberlite pipes. Journal of Geology 84: 673-684

Mitchell RH, Giuliani A, O'Brien H (2019) What is a kimberlite? Petrology and mineralogy of hypabyssal kimberlites. Elements 15: XXX-XXX

Moss S, Russell JK, Andrews GDM (2008) Progressive infilling of a kimberlite pipe at Diavik, Northwest Territories, Canada: insights from volcanic facies architecture, textures, and granulometry. Journal of Volcanology and Geothermal Research 174: 103-116

Pell J, Russell JK, Zhang S (2015) Kimberlite emplacement temperatures from conodont geothermometry. Earth and Planetary Science Letters 411: 131-141

Pittari A and 5 coauthors (2008) Eruption processes and facies architecture of the Orion Central kimberlite volcanic complex, Fort à la Corne, Saskatchewan; kimberlite mass flow deposits in a sedimentary basin. Journal of Volcanology and Geothermal Research 174: 152-170

Porritt LA, Russell JK, McLean H, Fomradas G, Eichenberg D (2013) A phreatomagmatic kimberlite: the A418 kimberlite pipe, NWT, Canada. In: Pearson DG and 6 coeditors (eds) Proceedings of 10th International Kimberlite Conference, Volume 2. Extended Abstract 10IKC-099

Price SE, Russell JK, Kopylova MG (2000) Primitive magma from the Jericho Pipe, N.W.T., Canada: constraints on primary kimberlite melt chemistry. Journal of Petrology 41: 789-808

Russell JK, Porritt LA, Lavallée Y, Dingwell DB (2012) Kimberlite ascent by assimilation-fuelled buoyancy. Nature 481: 352-356

Seropian G, Rust AC, Sparks RSJ (2018) The gravitational stability of lenses in magma mushes: confined Rayleigh-Taylor instabilities. Journal of Geophysical Research: Solid Earth 123: 3593-3607

Scott Smith BH (2008) The Fort à la Corne kimberlites, Saskatchewan, Canada: geology, emplacement and economics. Journal of the Geological Society of India 71: 11-55

Sparks RSJ and 6 coauthors (2006) Dynamical constraints on kimberlite volcanism. Journal of Volcanology and Geothermal Research 155: 18-48

Sparks RSJ (2013) Kimberlite volcanism. Annual Review of Earth and Planetary Sciences 41: 497-528

Spera FJ (1984) Carbon dioxide in petrogenesis III: role of volatiles in the ascent of alkaline magma with special reference to xenolith-bearing mafic lavas. Contributions to Mineralogy and Petrology 88: 217-232

Stone RS, Luth RW (2014) Orthopyroxene survival in deep carbonatite melts: implications for kimberlites. Contributions to Mineralogy and Petrology 171 doi: 10.1007/s00410-016-1276-2

FIGURE CAPTIONS

Figure 1. Kimberlite bodies in exposure and in cross section. (**A**) Igwisi Hills (Tanzania) kimberlite vent defined by a high-standing (<40 m) tephra cone and extra-crater lava overflowing the central volcano crater. AFTER BROWN ET AL. (2012). (**B**) Cross-section geology of the A418 kimberlite pipe (Diavik, Canada) showing pipe geometry, lithofacies complexity, and inferred original crater and vent geometry. Lithofacies abbreviations: MVK = massive volcaniclastic kimberlite; LVK = layered volcaniclastic kimberlite; CK = coherent kimberlite. MODIFIED FROM PORRITT ET AL. (2013).

Figure 2. Representative xenoliths and xenocrysts entrained by kimberlites. (**A**) Large, rounded mantle-derived peridotites, Bultfontein Mine (South Africa). PHOTO: J. ROBEY. (**B**) A large (~30 cm), well-rounded, smooth-surfaced, eclogite xenolith, Roberts Victor kimberlite (South Africa). PHOTO: B. SCOTT SMITH. (**C**) Characteristic millimetric ellipsoidal olivine

xenocrysts in a coherent kimberlite from Diavik (Canada). PHOTO: S. MOSS. (**D**) Characteristic centimetric ellipsoidal olivine xenocrysts in a kimberlite from Igwisi Hills (Tanzania). Photo: K. Russell. (**E**) Xenocrystic olivine (Ol) in kimberlite and a partially dissolved grain of orthopyroxene (Opx) from the Diavik kimberlite (Canada). PHOTO: C. BRETT. (**F**) Euhedral olivine from the Diavik kimberlite (Canada) showing late "phenocrystic" olivine overgrowth (arrows) on a sub-rounded xenocrystic core. PHOTO: C. BRETT.

Figure 3. Schematic hypothesis that kimberlite ascent is driven by assimilation-fuelled buoyancy. (A) Compositional evolution of proto-kimberlitic (i.e. carbonatitic) melts driven by assimilation of mantle silicate minerals and driving a chemically-induced exsolution of CO_2. Carbonatitic melts ($\lesssim$ 10–17 wt% SiO_2) assimilate Opx preferentially are enriched in SiO_2 to become kimberlite and ultimately reach olivine saturation. Increasing SiO_2 content also causes a concomitant drop in CO_2 solubility (see Inset B) causing exsolution of CO_2-dominated fluid and increasing magma buoyancy. (B) Compositional and pressure dependence of CO_2 solubility across the carbonate–silicate transition; changes in melt composition driven by silicate assimilation can cause a marked drop on CO_2 solubility. (**C**) Kimberlite evolution as a function of transport from the asthenospheric source, through the cratonic mantle lithosphere (CML), and crossing the graphite–diamond transition (D-G) zone before entering the crust (left panel). Dykes of carbonate-rich parent melt enter the CML and sample and entrain mantle xenoliths which disaggregate to release xenocrystic minerals which are variably assimilated causing exsolution and ultimately olivine crystallization (centre panel). The evolution of SiO_2 and CO_2 content (right panel) as a function of transport distance. CO_2 exsolution is initially chemical driven (i.e. assimilation) but then driven by decreasing pressure. Initially Opx and olivine are assimilated but continued SiO_2 enrichment allows for late stage crystallization of olivine.

Figure 4. Schematic illustrations of processes operating in an ascending kimberlite dyke presented in vertical cross-section views. A vertical pressure gradient (∇P) acts along the length of the dyke, which comprises a volatile-rich buoyant tip and melt-rich tail ascending through an elastic medium (with Young's modulus E and Poisson's ration ν). The dyke propagates in the direction of maximum compressive stress (σ_1) at a velocity of U, and its thickness (w) is aligned with the minimum compressive stress direction (σ_3). It is surrounded by a region of damaged host-rock (dashed region). In thickness/length view the dyke has a tear-drop profile shape, with a wide 'head' region (of length L_b) and pinched tail. In breadth/length view the dyke it has a pear-shaped geometry, as the breadth of the

buoyant volatile-rich tip is smaller than the melt-rich tail. Magma ascends rapidly in the dyke in a central jet that circulates and turbulently mixes the magma within. Volatile exsolution occurs due to depressurization and crystal assimilation, to feed the volatile-rich tip. Turbulent rounding by attrition of xenoliths and xenocrysts sourced from the damage zone occurs in the tip region.

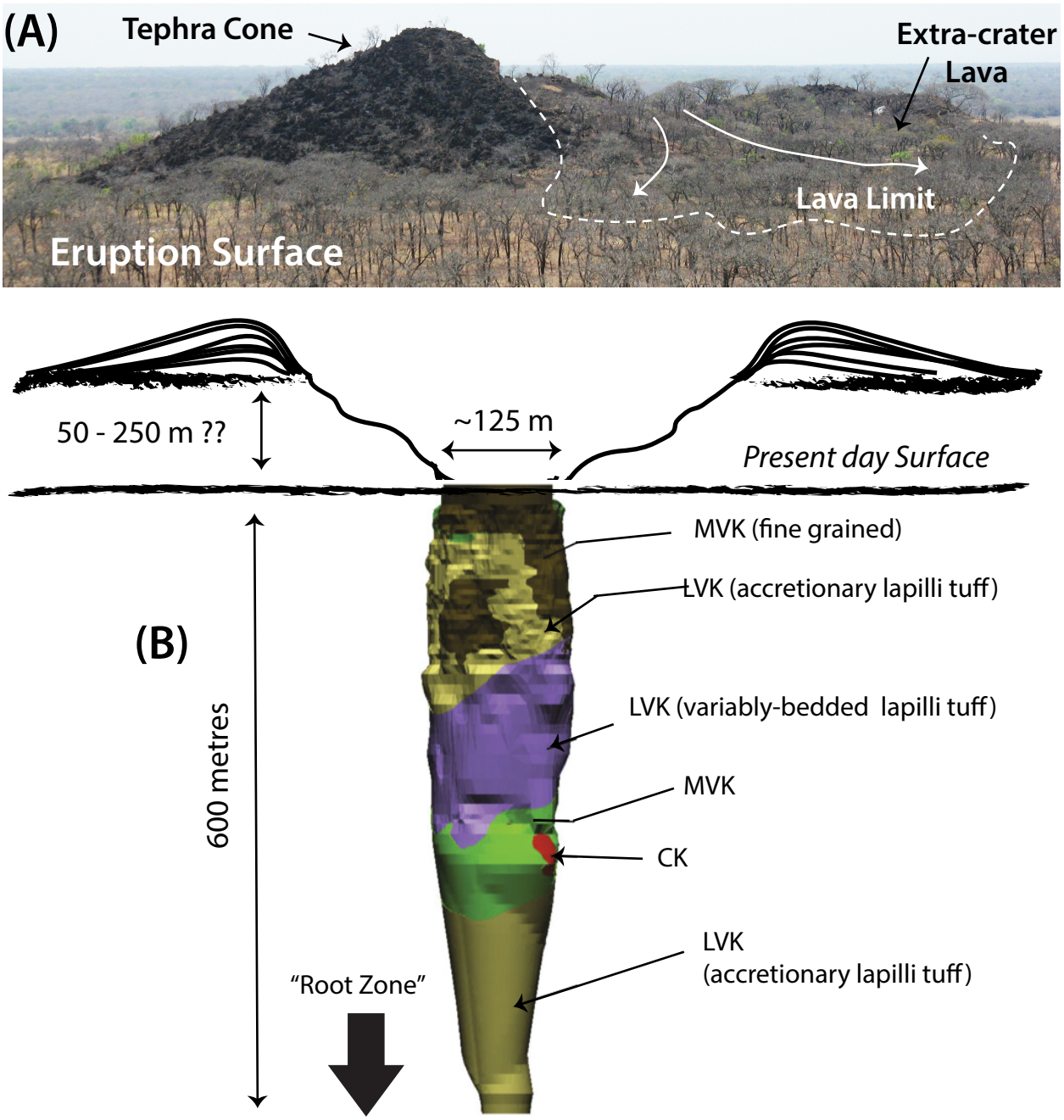

Figure 1. [Elements: Kimberlite - Chapter 6, 2019]

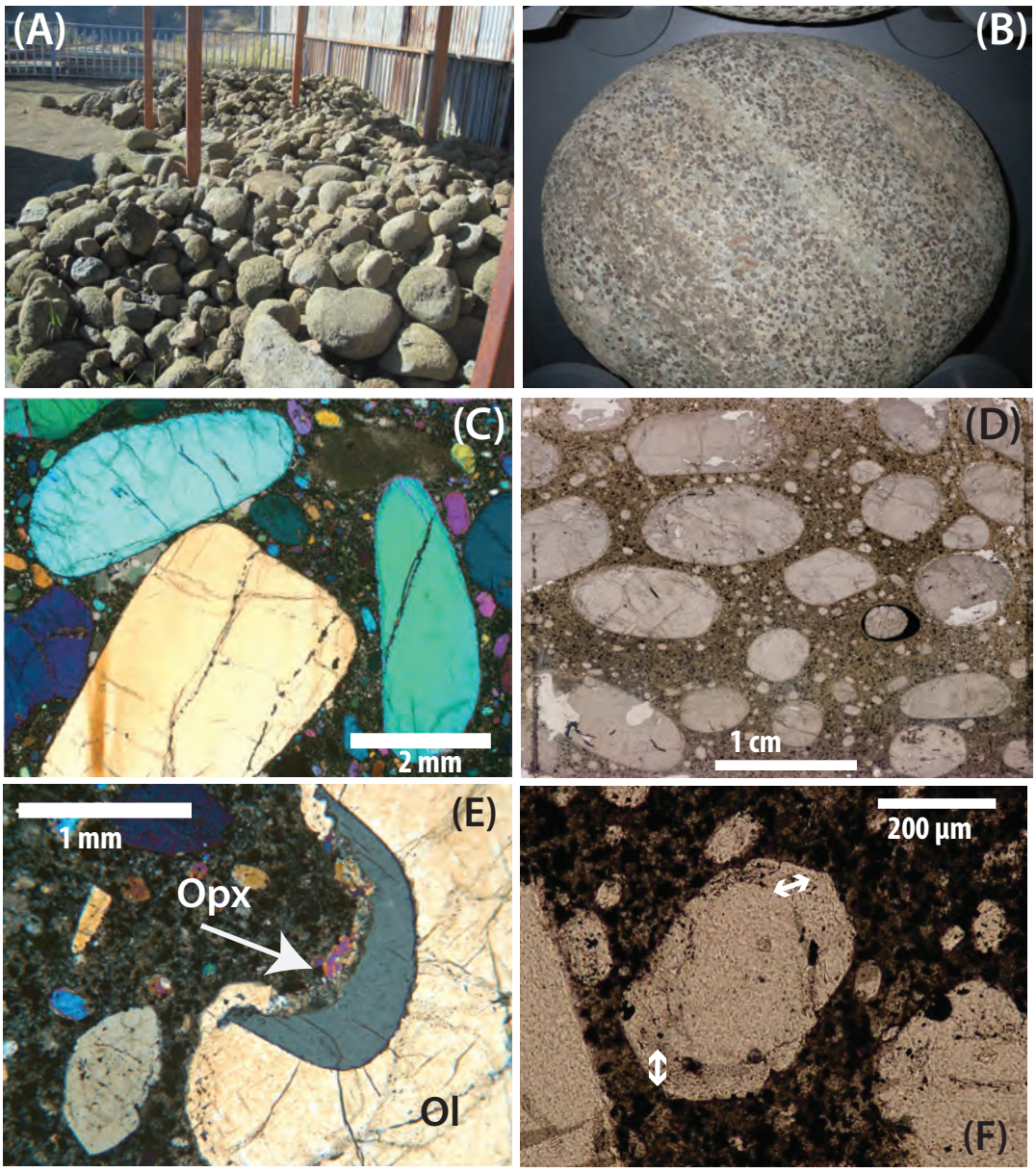

Figure 2. [Elements: Kimberlite - Chapter 6, 2019]

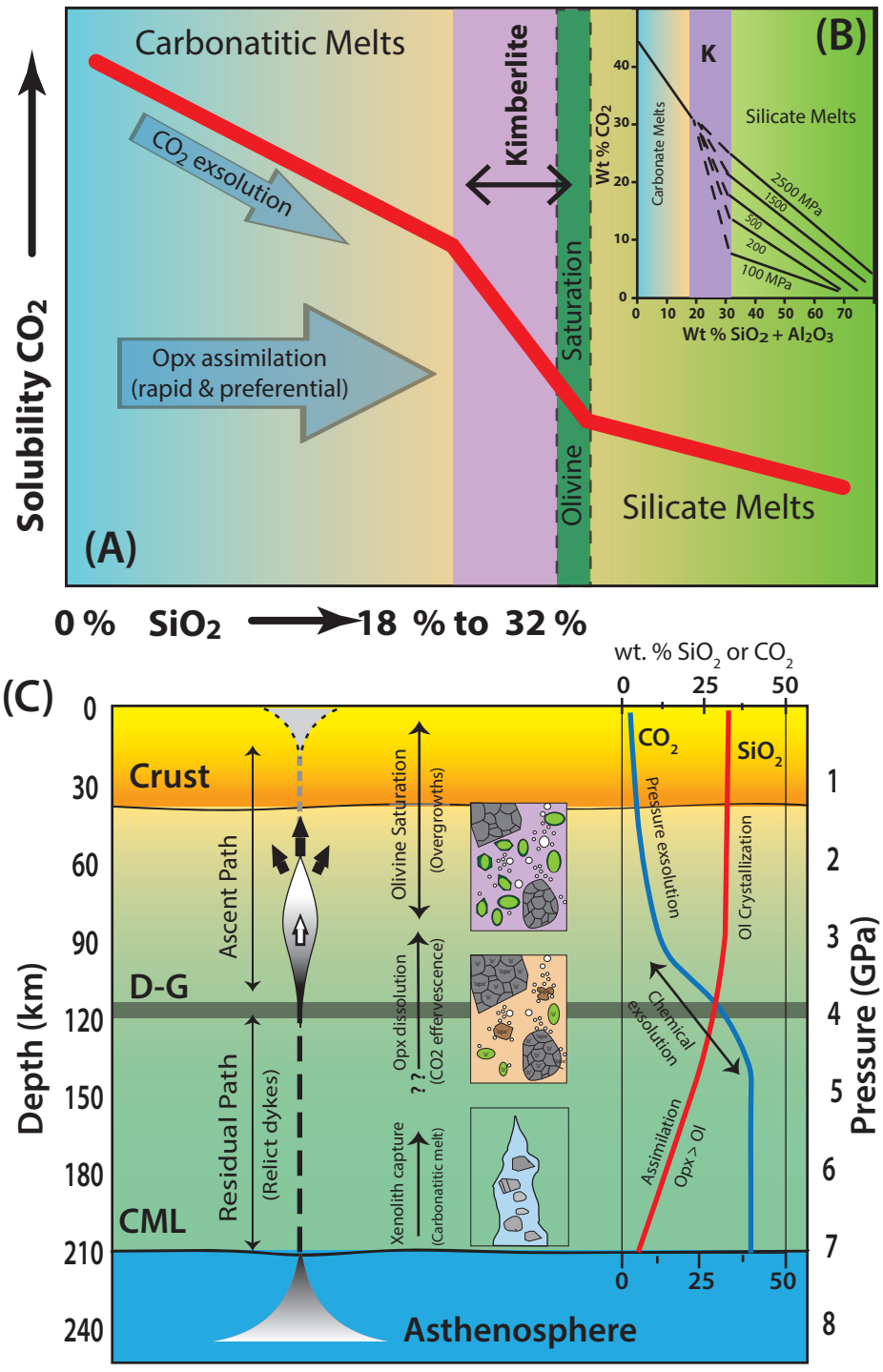

Figure 3. [Elements: Kimberlite - Chapter 6, 2019]

Kimberlite dyke cross-section view

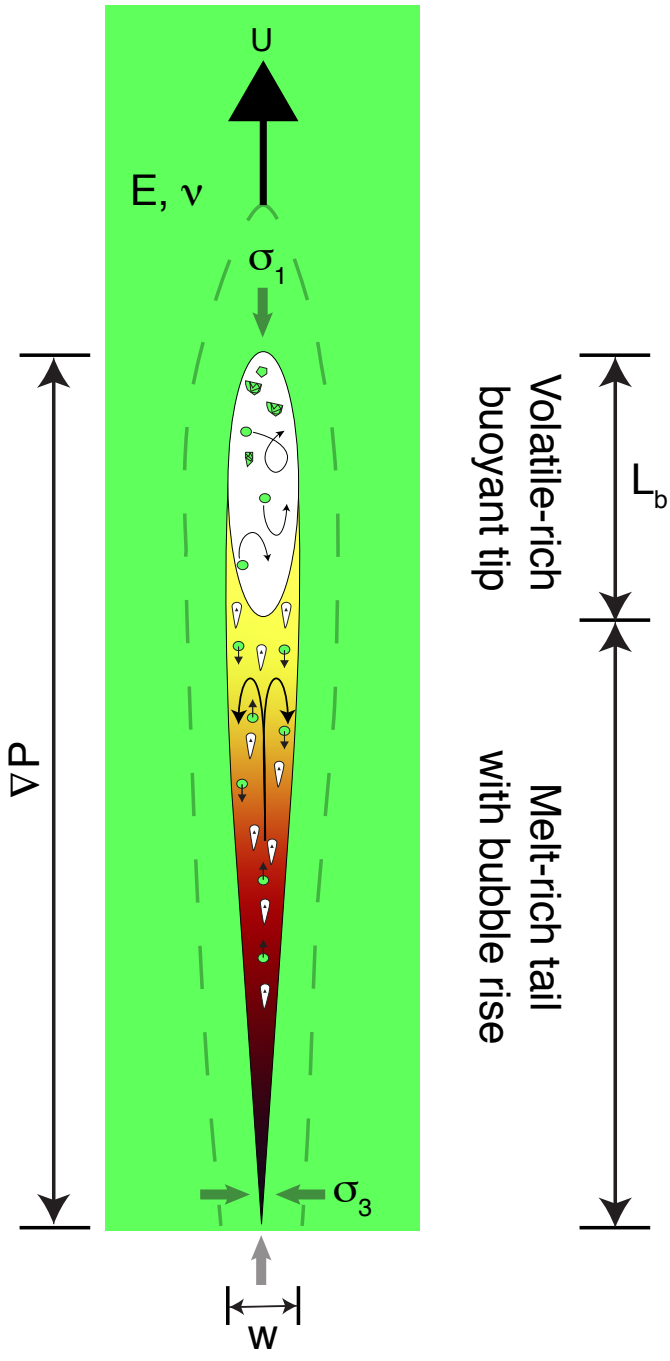

Kimberlite dyke plan view

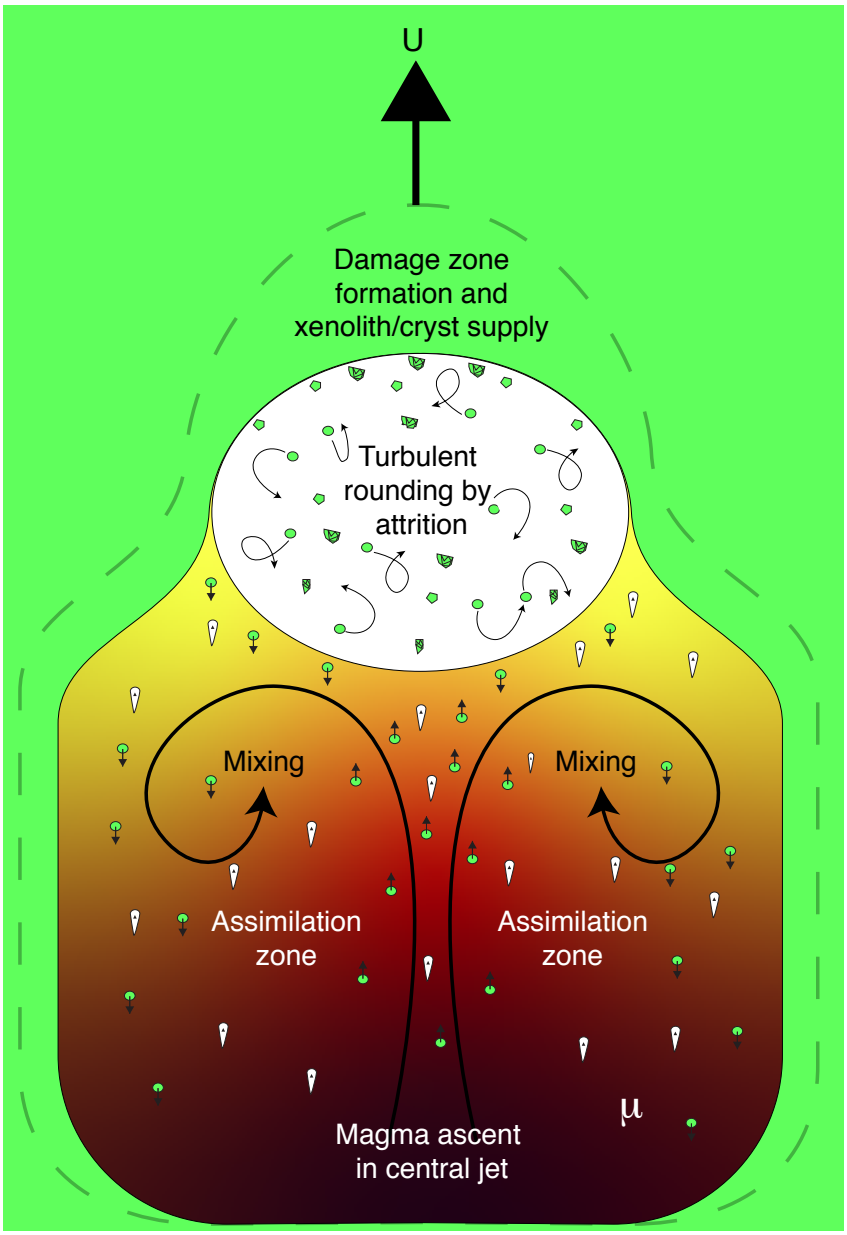

Continuous volatile exsolution due to depressurisation

Supplementary Material:

Kimberlite Volcanology: Transport, Ascent and Eruption

Kelly Russell[1], Steve Sparks[2] and Janine Kavanagh[3]

[1]University of British Columbia, Vancouver, Canada, V7W-2S1, krussell@eoas.ubc.ca; [2]Bristol University, Bristol, UK, BS8 1RJ; steve.sparks@bristol.ac.uk ; [3]University of Liverpool, Liverpool, UK, L69 3GP; Janine.Kavanagh@liverpool.ac.uk.

ADDITIONAL TEXT & REFERENCES ORGANIZED BY SUBHEADINGS

INTRODUCTION

Clement CR, Skinner EM, Scott Smith BH (1984) Kimberlite Redefined. Journal of Geology 92: 223-228

Hawthorne JB (1975) Model of a kimberlite pipe. Physics and Chemistry of the Earth 9: 1–15

McGetchin TR, Ullrich GW (1973) Xenoliths in maars and diatremes with inferences for the Moon, Mars, and Venus. Journal of Geophysical Research 78: 1833-1853

Mercier JC (1979) Peridotite xenoliths and the dynamics of kimberlite intrusion. *In* The Mantle Sample: Inclusions in kimberlites and other volcanics. American Geophysical Union 197-212

Wilson L, Head JW (2007) An integrated model of kimberlite ascent and eruption. Nature 447: 53-57

KIMBERLITE MELT AND MAGMA

Chepurov AA, Pokhilenko NP (2015). Experimental estimation of the kimberlite melt viscosity. Doklady Earth Sciences 462: 592-595

Kjarsgaard BA, Pearson DG, Tappe S, Nowell GM, Dowall DP (2009) Geochemistry of hypabyssal kimberlites from Lac de Gras, Canada: Comparisons to a global database and applications to the parent magma problem. Lithos 112: 236-248

Mitchell RH (1986) Kimberlites: Mineralogy, Geochemistry and Petrology 442pp.

Mitchell RH (2008) Petrology of hypabyssal kimberlites: Relevance to primary magma compositions. Journal of Volcanology and Geothermal Research 174: 1–8

Patterson M, Francis D, McCandless T (2009) Kimberlites: Magmas or mixtures? Lithos, 112: 191-200.

Persikov ES, Bukhtiyarova PG, Sokol AG (2018) Viscosity of haplokimberlitic and basaltic melts at high pressures: Experimental and theoretical studies. Chemical Geology 497: 54-63

Porritt L.A., Cas R.A.F., Schaefer B., McKnight S.W., (2012) Textural analysis of strongly altered kimberlite: Examples from the EKATI diamond mine, Northwest Territories, Canada. The Canadian Mineralogist 50: 625-641

Russell JK, Giordano G, Kopylova MG, Moss s (2006) Transport properties of Kimberlite. Kimberlite Emplacement Workshop, September, Saskatoon, Saskatchewan, 5 pp.

KIMBERLITE VOLCANOES

Kimberlite Pipe Infill

MVK is a homogeneous, structureless volcaniclastic rock containing mixtures of crystals, lapilli to coarse ash sized juvenile kimberlite pyroclasts, and lithic clasts. Local structures and heterogeneities include distorted intraclasts of layered rock and gas escape pipes. Primary textures and structures within MVK are commonly obscured by alteration wherein fine ash and primary pore space are partly or completely replaced or infilled by secondary alteration minerals, respectively. MVK deposits found as pipe infill have been interpreted as products of sustained explosive eruption within debris-filled pipes causing continous mixing of the pyroclastic materials, or resulting from column collapse during waning phases of eruption (Cas et al. 2008; Sparks 2013 for review).

LVK deposits are diverse and result from a variety of processes, eruptive styles, and depositional environments. They include fine to medium bedded tuffs, lapilli tuffs, lapillistones, and breccias and layers commonly dip into the pipe interior. Some LVK deposits likely formed in situ as primary pyroclastic deposits (i.e. pyroclastic flow, surge and fallout). Other LVK deposits are transported into the pipe from higher levels by subsidence or resedimentation of deposits from the crater or crater rim.

Dawson J (1994) Quaternary kimberlitic volcanism on the Tanzania Craton. Contributions to Mineralogy and Petrology 116: 473-485

Fontana G, MacNiocaill C, Brown RJ, Sparks RSJ, Field M (2011) Emplacement temperatures of pyroclastic and volcaniclastic deposits in kimberlite pipes in southern Africa. Bulletin of Volcanology 73:1063-1083

Gernon TM, Gilbertson MA, Sparks RSJ, Field M (2009) The role of gas fluidisation in the formation of massive volcaniclastic kimberlite. Lithos 112S: 438–51

Hayman PC, Cas RAF (2011) Criteria for interpreting kimberlite as coherent: insights from the Muskox and Jericho kimberlites. Bulletin of volcanology 73: 1005–1027

Kjarsgaard BA, Harvey SE, Du Plessis P, McClintock M, Zonneveld JP, Heaman L, McNeil D (2009) Geology of the Orion South kimberlite, Fort à la Corne, Canada. Lithos 112S:600–618

Kurszlaukis S, Lorenz V (2008) Formation of "Tuffisitic Kimberlites" by phreatomagmatic processes. Journal of Volcanology and Geothermal Research 174: 68-80

Lorenz V (1975) Formation of phreatomagmatic maar-diatreme volcanoes and its relevance to kimberlite diatremes. Physics and Chemistry of the Earth 9: 17–29

Moss S, Russell JK, Brett RC, Andrews GDM (2009) Spatial and temporal evolution of kimberlite magma at A154N, Diavik, Northwest Territories, Canada. Lithos 112: 541-552

Reid AM, Donaldson C, Dawson J, Brown R, Ridley W (1975) The Igwisi Hills extrusive "kimberlites": Physics and Chemistry of the Earth 9: 199-218

Scott-Smith, BH (2008) Canadian kimberlites: Geological characteristics relevant to emplacement. Journal of Volcanology and Geothermal Research 174: 9–19

Van Straaten BI, Kopylova MG, Russell JK, Scott Smith BH (2011) A rare occurrence of crater-filling clastogenic extrusive coherent kimberlite, Victor Northwest (Ontario, Canada). Bulletin of Volcanology 73:1047–62

RECONSTRUCTING KIMBERLITE ERUPTIONS [FALC -RELATED PAPERS]

Berryman AL, Scott Smith BH, Jellicoe BC (2004) Geology and diamond distribution of the 140/141 kimberlite, Fort à la Corne, central Saskatchewan, Canada. Lithos 76:99–114

Grunsky EC, Kjarsgaard BA (2009). Classification of distinct eruptive phases of the diamondiferous Star kimberlite, Saskatchewan, Canada based on statistical treatment of whole rock geochemical analyses. Applied Geochemistry 23:3321–3336

Harvey S, Kjarsgaard B, McClintock M, Shimell M, Fourie L, Du Plessis P, Read G (2009) Geology and evaluation strategy of the Star and Orion South kimberlites, Fort à la Corne, Canada. Lithos 112S:47–60

Kjarsgaard BA, Harvey SE, Zonneveld JP, Heaman LM, White D, McNeil D (2006) Volcanic stratigraphy, eruptive sequences and emplacement of the 140/141 Kimberlite, Fort a la Corne Field, Saskatchewan. Extended Abstract, 2006 Kimberlite Emplacement Workshop. Saskatchewan, Canada.

Kjarsgaard BA, Leckie DA, Zonneveld J-P (2007) Discussion of "Geology and diamond distribution of the 140/141 kimberlite, Fort a la Corne, central Saskatchewan, Canada". by A. Berryman, B.H. Scott Smith and B.C. Jellicoe (Lithos v. 76, p.99-114). Lithos 97, 422{428, 10.1016/j.lithos.2006.09.02.

Leahy, K. (1997). Discrimination of reworked pyroclastics from primary tephra-fall tuffs: a case study using kimberlites of Fort a la Corne, Saskatchewan, Canada. Bull Volcanol (1997) 59 :65–71.

Leckie DA, Kjarsgaard BA, Bloch J, McIntyre D, McNeil D, Stasiuk L, Heaman L (1997) Emplacement and reworking of cretaceous, diamond-bearing, crater facies kimberlite of central Saskatchewan, Canada. Geol Soc Am Bull 109:1000–1020

Pittari A, Cas RAF, Lefebvre N, Webb K, Kurszlaukis S (2006) Facies characteristics and architecture of Body 219 Fort a la Corne, Saskatchewan, Canada; implications for kimberlitic mass flow processes in a marine setting. Extended Abstracts, 2006 Kimberlite Emplacement Workshop. Saskatchewan, Canada.

Scott Smith BH, Smith SCS (2009) The economic implications of kimberlite emplacement. Lithos 112S:10–22

Scott Smith BH, Orr RG, Robertshaw P, Avery RA (1998) Geology of the Fort à la Corne kimberlites, Saskatchewan. In: Extended abstracts 7th international kimberlite conference, Cape Town, South Africa, pp 772–774

Zonneveld J-P, Kjarsgaard BA, Harvey Heaman LM, McNeil DH,Marcia KY (2004) Sedimentologic and stratigraphic constraints on emplacement of the star kimberlite, east-central Saskatchewan. Lithos 76:115–138

Zonneveld JP, Kjarsgaard BA, Harvey SE, McNeil D (2006) Accommodation space and kimberlite edifice preservation: implications for volcanological models of Fort a la Corne kimberlites. Extended Abstracts, 2006 Kimberlite Emplacement Workshop. Saskatchewan, Canada.

ENTRAINMENT AND MODIFICATION OF MANTLE CARGO

Decompression during kimberlite ascent induces internal stresses in xenoliths requiring volume expansion. High ascent rates imply rapid decompression rates that will exceed normal rates of ductile relaxation in xenoliths. The internal elastic stresses will accumulate promoting tensile failure to produce smaller xenoliths and xenocrysts. Residual stresses ($\Delta\sigma_R$) depend on ascent velocity (U), the bulk modulus (K_T) and viscosity (μ) of the xenolith, and the pressure drop over the ascent distance [$z - z_0$]:

$$\Delta\sigma_R = \rho\, g\, [z_0 - z] - K_T\, \frac{\rho g}{2\,\mu\, U}\, [z_0 - z]^2 \ . \quad \text{(S1)}$$

The velocity of the ascending magma dictates the time available for viscous relaxation. Equation S1 models the stress state mantle material (xenoliths and xenocrysts) as a function of transport distance (i.e. decompression) in an ascending magma as a function of ascent velocities. These stresses can then be compared to the tensile strengths of coarse and fine-grained peridotite or olivine grains.

Faster ascent rates dictate less viscous relaxation causing failure at smaller transport distances. Slower ascent allows longer times for viscous relaxation and therefore longer transport distances before olivine, for example, fractures. Any ascent velocity ≥1 m s^{-1} is sufficiently rapid to suppress viscous relaxation and the residual stresses are equal to the elastic limiting stresses. At these velocities the internal stresses in olivine rise to exceed the tensile strength of olivine after ~15 km of ascent (~4 h at 1 m s^{-1}); at these velocities the magma would transit 200 km in ~2 days. At lower velocities (e.g., 0.1 m s^{-1}), larger transport distances (22 km) are required to generate internal residual stresses exceeding the tensile strength of olivine.

Polymineralic rocks (e.g. peridotite) can have lower tensile strengths (σ) by a factor of ~5 than individual mineral grains (e.g., olivine). Coarse-grained rocks are generally weaker than fine-grained rocks ($\sigma \sim 100$ *vs*. 200 MPa, respectively). Thus, fine-grained mantle xenoliths, being stronger, are more likely to be transported intact. Olivine xenocrysts also undergo decompression-induced cracking recorded as sealed and healed cracks (Brett et al. 2015), but require more rapid decompression or greater transport distances to exceed their tensile strengths (~ 500 MPa).

Arndt NT, Guitreau M, Boullier AM, Le Roex A, Tommasi A, Cordier P, Sobolev A (2010) Olivine and the origin of kimberlite. Journal of Petrology 51: 573-602

Arndt NT, Boullier AM, Clement JP, Dubois M, Schissel D (2006) What olivine, the neglected mineral, tells us about kimberlite petrogenesis. eEarth 1: 15–21

Brett RC, Russell JK, Moss SW (2009). Origins of Olivine in Kimberlite: Phenocryst or Imposter? *Lithos* doi: 10.1016/j.lithos.2009.04.030.

Bussweiler Y, Foley SF, Prelević D, Jacob D (2015) The olivine macrocryst problem: New insights from minor and trace element compositions of olivine from Lac de Gras kimberlites, Canada. Lithos 220: 238-252

Giuliani A (2018) Insights into kimberlite petrogenesis and mantle metasomatism from a review of the compositional zoning of olivine in kimberlites worldwide. Lithos 312:322-342

Lensky NG, Niebo RW, Holloway JR, Lyakhovsky V, Navon O (2006) Bubble nucleation as a trigger for xenolith entrapment in mantle melts: Earth and Planetary Science Letters 245: 278-288

Mitchell RH, Carswell DA, Clarke DB (1980) Geological implications and validity of calculated equilibration conditions for ultramafic xenoliths from the pipe 200 kimberlite, northern Lesotho. Contributions to Mineralogy and Petrology 72: 205-217

Pilbeam LH, Nielsen T, Waight TE (2013) Digestion fractional crystallization (DFC): an important process in the genesis of kimberlites. Evidence from olivine in the Majuagaa kimberlite, southern West Greenland: Journal of Petrology 54: 1399-1425

Russell JK, Jones T, Andrews GDM, Edwards BR, Pell J (2017) Transport and eruption of mantle xenoliths: A lagging problem.11th International Kimberlite Conference Extended Abstract No. 11IKC-4626.

Roedder E, (1984) Fluid Inclusions: *In* Reviews in Mineralogy 12, Mineralogical Society of America 644 pp.

ASSIMILATION, VOLATILES, AND BUOYANCY

Brooker RA, Sparks RSJ, Kavanagh JL, Field M (2011) The volatile content of hypabyssal kimberlite magmas: some constrains from experiments on natural rock compositions. Bulletin of Volcanology 73:959–981

Canil D, Bellis AJ (2008) Phase equilibria in a volatile-free kimberlite at 0.1 MPa and the search for primary kimberlite magma. Lithos 105: 111-117

Fedortchouk Y, Canil D (2004) Intensive variables in kimberlite magmas, Lac de Gras, Canada and implications for diamond survival. Journal of Petrology 45: 1725-1745.

Kamenetsky VS, Grütter H, Kamenetsky MB, Gömann K (2013) Parental carbonatitic melt of the Koala kimberlite (Canada): Constraints from melt inclusions in olivine and Cr-spinel, and groundmass carbonate. Chemical Geology 353: 96-111

Kamenetsky VS, Yaxley GM (2015) Carbonate-silicate liquid immiscibility in the mantle propels kimberlite magma ascent. Geochemica et Cosmochimica 158: 48-56

Luth RW (2009) The activity of silica in kimberlites, revisited. Contributions to Mineralogy and Petrology 158: 283-294

Mitchell RH (1973) Composition of olivine, silica activity and oxygen fugacity in kimberlite. Lithos 6: 65-81

Moussallem Y, Morizet Y, Massuyeau M, Laumonier M, Gaillard F (2015) CO_2 Solubility in kimberlite melts. Chemical Geology 418: 198-205

Russell JK, Porritt L, Hilchie L (2013) Kimberlite: Rapid ascent of lithospherically modified carbonatites. *In*: D. G. Pearson et al. (eds.) Journal Geological Society India 1: 195-210

Stamm, N. and Schmidt, M. (2017) Asthenospheric kimberlites: Volatile contents and bulk compositions at 7 GPa. Earth and Planetary Science Letters 474: 309-321
White JL, Sparks RSJ, Bailey K, Barnett WP, Field M, Windsor L (2012) kimberlite sills and dykes associated with the Wesselton kimberlite pipe, kimberley, South Africa. South African Journal of Geology 115: 1-32

KIMBERLITE TRANSPORT IN DYKES [KIMBERLITE DYKE THEORY]

The main driver for dyke ascent is magma buoyancy, expressed by the buoyancy pressure P_b (Lister and Kerr, 1991):

$$P_b = \Delta\rho\ g\ h \qquad (S2)$$

where $\Delta\rho$ is the density contrast between magma and host-rock, h is the ascent distance, and g is gravity. When the dyke remains connected to its source at depth and $\Delta\rho$ is 200 kg m^3, the buoyancy pressure along 150 km of dyke will be 300 MPa (Eq. S2).

Dykes are kept open by an elastic overpressure P_e:

$$P_e = \sim \frac{m\ w}{l} \qquad (S3)$$

where w is the dyke thickness, l is its cross-sectional width, and m is the stiffness of the host-material, which is governed by the Young's modulus E and the Poisson's ratio ν:

$$m = \frac{E}{(1 - \nu)} \qquad (S4)$$

For E = 40 GPa, ν = 0.2, and w/l of 6 x 10^{-4} (w = 0.6 m; l = 1 km) the elastic pressure is ~30 MPa.

A tear-drop shaped geometry develops (Takada 1990) once the dyke exceeds the buoyant length L_b (Fig. 4; Taisne and Tait 2009):

$$L_b = \left(\frac{K_c}{\Delta\rho\ g}\right)^{\frac{2}{3}} \qquad (S5)$$

where K_c is the fracture toughness (~ 2 x 10^7 Pa $m^{1/2}$). For proto-kimberlite magma ascending from 150 km depth, the buoyant length of a kimberlite dyke is ~465 m. In the shallow crust this buoyant length would shorten to ~160 m because volatile exsolution will increase $\Delta\rho$ (~1000 kg m^{-3}).

Assuming a tear-drop model geometry (Fig. 4) for kimberlite dykes implies a cross-sectional dyke area of ~400 m^2, assuming l is equivalent to L_b, w is 1 m and $\Delta\rho$ is 200 kg m^{-3}. The overall volume of the 150 km long dyke would then be ~5x10^7 m^3.

The dynamics of magma flow are expressed by the Reynold's number:

$$Re \equiv \frac{\rho_{liq}\, U\, w}{\mu} \qquad (S6)$$

Where ρ_{liq} is the density of the magma, U is the characteristic velocity, and μ is the magma viscosity. High Reynold's number indicates dominance of inertial forces over viscous forces, and for the case of kimberlite dykes this is due to inferred rapid ascent velocity. The low viscosity of kimberlite melt (< 1 Pa s) means it is highly likely that the flow will have a high Reynold's number and be turbulent. Following Sparks et al. (2006) a characteristic turbulent magma velocity can be calculated for the upward flow of kimberlite:

$$U = 7.7 \left(\frac{(w/2)^5}{\mu\,(\rho_{\mathrm{liq}} g \Delta\rho)^3}\right)^{\frac{1}{7}} g\Delta\rho \qquad (S7)$$

Where μ is the melt viscosity, ρ_{liq} is the magma density, g is gravity, $\Delta\rho$ is the local density difference, and *w* is the dyke thickness. For proto-kimberlite melt viscosity of 6-36 x 10^{-3} Pa s, magma density of 2800 kg m^{-3}, average dyke width of 0.1-1 m, and density difference of 200-1000 kg m^{-3}, calculated magma velocities are ~20-90 m/s.

Ferguson J, Martin H, Nicolaysen LO, Danchin RV (1975) Gross Brukkaros: A kimberlite-carbonatite volcano. Physics and Chemistry of the Earth 9: 219-234

Jelsma H, Barnett W, Richards S, Lister G (2009) Tectonic setting of kimberlites. Lithos 112S: 155-165

Kavanagh JL (2018) Mechanisms of magma transport in the upper crust – Dyking. *In*: S. Burchardt (ed) Volcanic and Igneous Plumbing Systems. 55-88

Kavanagh JL, Menand T Sparks RSJ (2006) An experimental investigation of sill formation and propagation in layered elastic media. Earth and Planetary Science Letters 245: 799-813.

Kavanagh, JL, Sparks RSJ (2009) Temperature changes in ascending kimberlite magma. Earth and Planetary Science Letters 286: 404-413

Kavanagh, JL, Sparks RSJ (2011) Insights of dyke emplacement mechanics from detailed 3D dyke thickness datasets. Journal of the Geological Society 168: 965-978

Lister JR, Kerr RC (1991) Fluid-mechanical models of crack propagation and their application to magma transport in dykes. Journal of Geophysical Research 96:10049–77

Menand T, Tait SR (2001) A phenomenological model for precursor volcanic eruptions. Nature 411, 678–680

Rubin AM (1995) Propagation of magma-filled cracks. Annual Review of Earth and Planetary Sciences 23: 287-336

Sparks RSJ, Baker L, Brown RJ, Field M, Schumacher J, Stripp G, Walters A (2006) Dynamical constraints on kimberlite volcanism. Journal of Volcanology and Geothermal Research 155: 18-48

Taisne B, Tait S (2009) Eruption versus intrusion? arrest of propagation of constant volume, buoyant, liquid-filled cracks in an elastic, brittle host. Journal of Geophysical Research 114: 1–7

Takada, A. (1990) Experimental study on propagation of liquid-filled crack in gelatin: Shape and velocity in hydrostatic stress condition. Journal of Geophysical Research: Solid Earth, 95(B6), 8471-8481

Vergniolle S, Jaupart C (1986) Separated two-phase flow and basaltic eruptions. Journal of Geophysical Research 91: 12842-12860

KIMBERLITE MELT PRODUCTION AND TRIGGERING

Here we apply the recent process-oriented models for the segregation and ascent of kimberlite melt. We assume ascent is the consequence of low viscosity buoyant proto-kimberlite melt separating from the asthenosphere and accumulating at the base of the lithosphere. In such circumstances a key boundary is the solidus of the mantle, which for our purposes defines the lithosphere-asthenosphere boundary separating permeable regions with melt present and impermeable regions without melt (Jackson et al. 2018). Melts separating from the asthenosphere by porous flow accumulate as a buoyant melt-rich layer beneath the boundary and we infer that such layers source kimberlites. Time scales for ascent therefore depend on the dimensions of this layer, its growth rate and development of buoyancy-induced instabilities.

We use models of Rayleigh Taylor (RT) instabilities, where a thin buoyant layer of low viscosity melt grows at rate $\dot{h}$ beneath high viscosity mantle lithosphere (Seropian et al. 2018). The fastest growing wavelength, λ, is given by:

$$\lambda = 9.058 \left[\frac{\dot{h}}{g\,\Delta\rho}\right]^{1/2} \mu_1^{\,-1/6}\, \mu_2^{\,2/3} \qquad \text{(S8)}$$

where μ_1 is the viscosity of the melt layer (~3 x 10^{-2} Pa s; Dobson et al. 1996), μ_2 is the mantle lithosphere viscosity and Δρ is the density difference between the melt layer and overlying mantle. Mantle viscosity depends strongly on temperature, OH-content and mineralogy, and we adopt a value ~$10^{20\pm1}$ Pa s. We assume Δρ of 300 kg/m^3. Approximate values of $\dot{h}$ for the supply of proto-kimberlite melt derive from two plausible conceptual models. If we assume melt results from 0.1% partial melting, a mantle plume with a rise speed of 0.1 m/y (Steinberger and Atretter, 2009) yields a 1-D melt flux ($\dot{h}$) of 10^{-4} m/y and would imply a λ of 11,556 km. Conversely, a passive compaction model for melt extraction (Mackenzie 1985) yields an estimated accumulation rate of ~ 10^{-5} m/year and λ of 3,654 km. However, these wavelengths are much greater than kimberlite cluster footprints and thus it seems that equation (S8) results in geologically and physically unlikely results.

We thus turn to a model (Seropian et al. 2018) of instability from confined layers where the width of the layer is much less than λ. There is a simple linear scaling of the actual horizontal dimension of the buoyant layer, D, to λ with time (see Seropian et al. 2018). A representative time scale for exponential growth is:

$$\tau_c = \frac{\mu_2}{[0.053\; g\;\Delta\rho\; D]} \qquad (S9)$$

and is the time it takes for a small perturbation to grow in height by a factor of e (i.e. ≈ 2.72). The physics of the instability for magma ascent is not, however, captured in equation S9, but we expect τ_c to scale with the instability time through the following arguments. As previously discussed kimberlite ascent through the lithosphere is along dykes, so an RT instability must develop conditions for brittle failure. As an RT instability grows in height there will be an overpressure that increases with height. Further for exponential growth (see Figure 6 in Seropian et al. 2018) tensional strain rate along the melt mantle boundary increases with time. Both of these changes can lead to eventual failure with nucleation and growth of a dyke. A process model of these processes has yet to be developed, but the instability timescale should scale as indicated by equation S9. Thus to get an order of magnitude sense of the frequency of kimberlite ascent and magma volumes we calculate values of τ_c.

A critical layer thickness, h, can be calculated from τ_c and $\dot{h}$ for different values of D. A volume of magma, V_m, is calculated assuming cylindrical geometry from $\pi h(D/2)^2$. Values of D may reflect either ponding in inverted depressions along an irregular topographic base to the lithosphere or be dictated by spacing of deep lithospheric structures that facilitate melt ascent. Based on typical scales of kimberlite vent clusters, and to generate time scales similar to the observed rates, we assumed D values of 300 and 30 km, which return timescales of 68 to 680 ky, respectively. A background melt accumulation rate ($\dot{h}$) of 10^{-5} m/year implies corresponding thicknesses (h) of 0.68 and 6.8 m and volumes of 48 and 4.8 km^3 at these trigger times. These volumes are up to an order of magnitude higher than volumes of individual kimberlites ($3.5x10^{-3}$ to 1 km^3). However, there are many uncertainties in the choices of model input parameters. Furthermore a significant volume (>80%) of the magma generated could be intruded rather than erupted. Thus the difference in results are not regarded as problematic.

Future models of melt layer instability and dyke nucleation need to be developed that can be reconciled with kimberlite erupted volumes as well as rates of kimberlite events.

de Bremond d'Ars J, Jaupart C, Sparks RSJ (1995) Distribution of volcanoes in active margins. Journal of Geophysical Research 100: 20421-20432

Griffin WL, Batumike JM, Greau Y, Pearson NJ, Shee SR, O'Reilly S.Y. (2014) Emplacement ages and sources of kimberlites and related rocks in southern Africa: U–Pb ages and Sr–Nd isotopes of groundmass perovskite. Contributions to Mineralogy and Petrology 168: 1032

Heaman LM, Kjarsgaard BA, Creaser RA (2003) The timing of kimberlite magmatism in North America: implications for global kimberlite genesis and diamond exploration. Lithos 71: 153-184

Heaman LM, Kjarsgaard BA (2000) Timing of eastern North American kimberlite magmatism: continental extension of the Great Meteor hotspot track? Earth Planetary Science Letters 178: 253-268

James TS, Gowan EJ, Wada I, Wang K (2009) Viscosity of the asthenosphere from glacial isostatic adjustment and subduction dynamics at the northern Cascadia subduction zone, British Columbia, Canada. Journal of Geophysical Research 114: B04405

Jackson M, Blundy J, Sparks RSJ (2018) Chemical differentiation, cold storage and remobilization of magma in the Earth's crust. Nature 564:405-409
Katz RF, Spiegelman M, Holtzman B (2006) The dynamics of melt and shear localization in partially molten aggregates. Nature 442: 676-9
Lockhart G, Grutter H, Carlson J (2004) Temporal, geomagnetic and related attributes of kimberlite magmatism at Ekati, Northwest Territories, Canada. Lithos 77: 665-682
Mackenzie D (1985) The extraction of magma from the crust and mantle. Earth and Planetary Science Letters 74: 81-91
O'Neill CJ, Lenardic A, Griffen WL, O'Reilly SY (2008) Dynamics of cratons in an evolving mantle. Lithos 102: 12-24
Steinberger B, Antretter M (2009) Conduit diameter and buoyant rising speed of mantle plumes: Implications for the motion of hot spots and shape of plume conduits. Geochemistry, Geophysics, Geosystems 7:11
Whitehead JA, Luther D (1975) Dynamics of laboratory diapir and plume models. Journal of Geophysical Research 80: 705–717
Zonneveld J-P, Kjarsgaard BA., Harvey SE, Heaman LA, McNeil DH, Marcia KY (2004) Sedimentologic and stratigraphic constraints on emplacement of the Star Kimberlite, east–central Saskatchewan. Lithos 76: 115-138

THE END